Thermal quenching of chromium photoluminescence in ordered perovskites. II. Theoretical models

R. H. Bartram and J. C. Charpie
Department of Physics and Institute of Materials Science, University of Connecticut, Storrs, Connecticut 06268

L. J. Andrews and A. Lempicki*
GTE Laboratories, Inc., Waltham, Massachusetts 02254
(Received 18 February 1986)

Several theoretical models for thermal quenching of chromium photoluminescence in ordered perovskites, whose parameters are severely constrained by empirical spectral information, are compared. Models based on linear coupling to modes of a_{1g} symmetry fail by 6—8 orders of magnitude to explain the observed radiationless-transition rate. A new model, which combines linear coupling to an a_{1g} mode with quadratic coupling to a t_{2g} mode, is in order-of-magnitude agreement with experiment.

I. INTRODUCTION

The data on $^4T_{2g} \rightarrow {}^4A_{2g}$ fluorescence of low-field chromium complexes, reported in the preceding paper[1] (henceforth designated I), present a singular theoretical challenge. Interest in the theory of radiationless transitions has accelerated rapidly in recent years. Much of the formalism was developed initially for color centers in ionic crystals,[2] and subsequently applied to a wide range of phenomena, including internal conversion and intersystem crossing in molecules, thermal ionization and recombination, energy transfer, paramagnetic relaxation, diffusion, recombination-enhanced defect reactions and intrinsic defect formation.[3,4] The present discussion focuses on radiationless deactivation of ions in solids. Although the theory has been eminently successful in elucidating trends,[5,6] absolute quantitative tests have been relatively rare. The present investigation provides an opportunity for such a test, in a context of some technological significance.

Radiationless processes in transition-metal complexes have been relatively neglected, with some notable exceptions. Englman and Barnett[7] and Struck and Fonger[8] have investigated high-field chromium complexes (ruby and emerald). The latter employed a single-configuration-coordinate model with combined linear and quadratic coupling which incorporated a number of adjustable parameters including the phonon frequency. They found that the adjusted phonon frequency required to fit radiationless transition rates was substantially larger than that required to fit optical line shapes. Tamimura *et al.* have applied a similar model to Cu^+ in $RbMgF_3$.[9] Sturge[10] employed the multimode, linear-coupling theory of Pryce[11] to explain radiationless transition rates of Co^{2+} in $KMgF_3$; a residual discrepancy was attributed to anharmonicity.

The object of the present investigation is to achieve a quantitative understanding of the factors which govern the quantum efficiency of fluorescence in low-field chromium complexes. To that end, several theoretical models are examined in which the parameters are severely constrained by experimental data on the temperature dependence of photoluminescence spectra and lifetimes, presented in I. A preliminary account of this work has been published in a conference proceedings.[12] The theory of radiationless transitions is reviewed concisely in Sec. II. The promoting interaction is considered in Sec. III, with particular emphasis on the conjectured role of promoting-mode selection rules.[13] A single-configuration-coordinate, linear-coupling model is presented in Sec. IV, and is generalized to a multimode, linear-coupling model in Sec. V. The combined effects of linear coupling to a symmetric (a_{1g}) mode and quadratic coupling to an asymmetric (t_{2g}) mode are explored in Sec. VI. Finally, the various models are compared and evaluated in Sec. VII.

II. THEORY OF RADIATIONLESS TRANSITIONS

Radiationless transitions can only occur between nonstationary states of a system; thus the radiationless transition rate depends critically on the sort of nonstationary state which is prepared in a given experiment.[14] In the adiabatic-coupling scheme, radiationless transitions are presumed to occur between Born-Oppenheimer states $\Psi_{n\nu}(r,Q)$, given by

$$\Psi_{n\nu}(r,Q)=\phi_n(r,Q)\theta_{n\nu}(Q) , \tag{1}$$

where $\phi_n(r,Q)$ is an eigenfunction of the electronic Hamiltonian $H_e(Q)$ for fixed nuclear coordinates Q,

$$H_e(Q)=T_E+V(r,Q) , \tag{2}$$

$$H_e(Q)\phi_n(r,Q)=U_n(Q)\phi_n(r,Q) . \tag{3}$$

The electronic eigenvalue $U_n(Q)$ then serves as the potential energy of interaction of the nuclei;

$$[T_N+U_n(Q)]\theta_{n\nu}(Q)=E_{n\nu}\theta_{n\nu}(Q) . \tag{4}$$

In these equations, r and Q denote, respectively, all elec-

tronic coordinates and all symmetry-adapted combinations of nuclear coordinates, and T_E and T_N are the respective electronic- and nuclear-kinetic-energy operators.

Radiationless transitions between Born-Oppenheimer states of the same multiplicity (internal conversion) are mediated by the nonadiabaticity operator, defined by

$$H_{\mathrm{NA}}\Psi_{n\nu}=(H-E_{n\nu})\Psi_{n\nu}=[T_N,\phi_n]\theta_{n\nu}\,. \tag{5}$$

The radiationless transition rate, W_{NR}, between electronic states i and f is obtained in first-order, time-dependent perturbation theory by summing over final vibrational states and thermally averaging over initial vibrational states. It is convenient to distinguish between promoting modes which mix the initial and final electronic states, and accepting modes which absorb the difference in electronic energy.[15] In systems of high symmetry, such as octahedral chromium complexes, promoting and accepting modes are distinct and one can write the vibrational wave function in the form

$$\theta_{n\nu}(Q)=\left[\prod_p \chi_{n\nu_p}(Q_p)\right]\left[\prod_a \chi_{n\nu_a}(Q_a)\right], \tag{6}$$

where Q_a and Q_p are symmetry-adapted normal coordinates for accepting and promoting modes, respectively. Bartram and Stoneham[16] have obtained the following convenient approximation for W_{NR}, applicable to this case:

$$\begin{aligned}W_{\mathrm{NR}}=(2\pi/\hbar)\sum_p |\langle\phi_f(Q_0)|\partial H_e/\partial Q_p|\phi_i(Q_0)\rangle|^2 \\ \times\sum_\alpha\sum_\beta\left[P_\alpha|\langle\chi_{f\beta_p}|Q_p|\chi_{i\alpha_p}\rangle|^2\right. \\ \times\left[\prod_a|\langle\chi_{f\beta_a}|\chi_{i\alpha_a}\rangle|^2\right] \\ \left.\times\delta(E_{f\beta}-E_{i\alpha})\right],\end{aligned} \tag{7}$$

$$P_\alpha=\exp(-E_{i\alpha}/k_BT)/\sum_\gamma\exp(-E_{i\gamma}/k_BT)\,, \tag{8}$$

where Q_0 denotes the equilibrium lattice configuration. Within the harmonic approximation, this expression for W_{NR} in the adiabatic-coupling scheme is formally identical with that appropriate to the static-coupling scheme,[17,18] in which the electronic wave functions are independent of Q and radiationless transitions are mediated by off-diagonal elements of the potential-energy operator; this equivalence was demonstrated previously for more idealized models.[19–21] Equation (7) avoids the recently discredited "Condon" approximation for radiationless transitions, first introduced by Huang and Rhys,[2] which has now been shown by Huang to underestimate transition rates by three orders of magnitude.[19] Further simplification of Eq. (7) can be achieved by exploiting well-known properties of harmonic-oscillator wave functions, with the result

$$W_{\mathrm{NR}}=\sum_p\nu_p\omega_p[(\bar{n}_p+1)G(\Omega_0-\omega_p)+\bar{n}_pG(\Omega_0+\omega_p)]\,, \tag{9}$$

where ω_p is the angular frequency of promoting mode p, $\bar{n}_p$ is its phonon occupation number,

$$\bar{n}_p=[\exp(\hbar\omega_p/k_BT)-1]^{-1}\,, \tag{10}$$

$\hbar\Omega_0$ is the energy gap between electronic states in their respective equilibrium configurations, and the factor ν_p incorporates the promoting interaction,

$$\nu_p=(\pi/\hbar\omega_p^2)|\langle\phi_f(Q_0)|\partial H_e/\partial Q_p(Q_0)|\phi_i(Q_0)\rangle|^2\,. \tag{11}$$

The normalized line-shape function $G(\Omega)$ is given in terms of accepting-mode vibrational overlap integrals by

$$\begin{aligned}G(\Omega)=\prod_a\sum_{\alpha_a}\sum_{\beta_b}P_{\alpha_a}|\langle\chi_{f\beta_a}|\chi_{i\alpha_a}\rangle|^2 \\ \times\delta(\Omega_{f\beta_a}-\Omega_{i\alpha_a}+\Omega_0-\Omega)\,,\end{aligned} \tag{12}$$

where $E=\hbar(\Omega_0+\Omega)$. The function $G(\Omega)$ also occurs in spectral line shapes for radiative transitions; however, it is evident from Eq. (9) that the radiationless-transition rate involves this function for values of its argument very far from the range of values accessible to direct observation. Reliable evaluation of this line-shape function is the central problem in application of the theory of radiationless transitions. Its exact form depends on the model assumed for accepting-mode interactions; an exploration of alternative models is the agenda of subsequent sections. For a center of sufficiently high symmetry that promoting and accepting modes are distinct, evaluation of the promoting-mode factors ν_p can be considered independently of the line-shape function.

III. PROMOTING INTERACTION

The promoting interaction which mixes initial and final electronic states is incorporated in the factors ν_p, defined by Eq. (11), which are treated as constants. Only promoting modes of t_{1g} symmetry can mix $^4A_{2g}$ and $^4T_{2g}$ electronic states. The absence of possible t_{1g} distortions of the seven-atom octahedron comprising the chromium ion and its immediate ligands has inspired the speculation that promoting-mode selection rules[13] are operative in these complexes. However, normal modes of elpasolite have been derived by Lentz[22] in the zero-wave-vector approximation in terms of symmetry-adapted displacements within the ten-atom primitive unit cell. These include degenerate normal modes of t_{1g} symmetry involving counter-rotating displacements of anion octahedra about trivalent and monovalent cations, as shown in Fig. 1, which are fully effective in promoting radiationless transitions. We will also adopt the same zero-wave-vector approximation, and assume a single set of degenerate promoting modes; accordingly, we will drop the summation in Eq. (9).

Spin-orbit interaction splits the $^4T_{2g}$ term into four fine-structure levels $E'(\Gamma_7)$, $E''(\Gamma_6)$, and $2\,U'(\Gamma_8)$, and the $^4A_{2g}$ term transforms as $U'(\Gamma_8)$.[23] Matrix elements of components of the promoting-mode crystal potential $V_i(t_{1g})$ $[=\partial H_e/\partial Q(t_{1g})]$ in the coupled representation

are expressed in terms of reduced matrix elements in the uncoupled representation by exploiting the point-group analogue of the Wigner-Eckart theorem:[24]

$$\langle U'\alpha \mid V_i(t_{1g}) \mid \Gamma\beta\sigma\rangle = \sum_a \sum_b \langle A_{2g}||V(t_{1g})||T_{2g}\rangle \times\langle T_1T_2ib \mid A_2\rangle \times\langle U'A_2a \mid U'\alpha\rangle \times\langle U'T_2ab \mid \Gamma\beta\sigma\rangle , \quad (13)$$

where $i=x,y,z$ labels rows of the t_{1g} representation. The last three factors on the right-hand side of Eq. (13) are tabulated point-group equivalents of Clebsch-Gordon coefficients.[23]

Squares of matrix elements were averaged over magnetic substates of initial fine-structure levels and summed over final substates. In this manner, it was established that the radiationless-transition rate is independent of fine-structure level, with the consequence that no additional temperature dependence is introduced by spin-orbit splitting. The reduced matrix element in Eq. (13) was evaluated for a special case, with the result

$$\langle A_2||V(t_{1g})||T_2\rangle = \sqrt{3}\langle \zeta \mid V_z(t_{1g}) \mid v\rangle , \quad (14)$$

where t_{2g} orbitals are designated as ξ,η,ζ and e_g orbitals as u,v. It then follows from Eqs. (11), (13), and (14) that the promoting-mode factor ν is given by

$$\nu = (\pi/M\hbar\omega_p^2) \mid \langle \zeta \mid V_z(t_{1g}) \mid v\rangle \mid^2 , \quad (15)$$

where the factor M, the mass of one halogen ion, arises from the conversion of mass-weighted coordinates.

In order to obtain a crude estimate of the promoting-mode factor ν, the matrix element in Eq. (15) was evaluated with free-atom d orbitals expanded in a Gaussian basis,

$$\zeta = 2xyf(r) , \quad (16)$$

$$v = (x^2-y^2)f(r) , \quad (17)$$

$$f(r) = \sum_{k=1}^{4} C_k[(2\zeta_k)^7/\pi^3]^{1/4}\exp(-\zeta_k r^2) , \quad (18)$$

where C_k and ζ_k are tabulated.[25] Bartram and Stoneham[16] have emphasized the importance of employing the exact potential in Eq. (11) rather than a pseudopotential such as the point-ion potential.[26] The potential corresponding to a unit azimuthal displacement of four ligand nuclei (each nucleus displaced by $\frac{1}{2}$ Bohr) is

$$V_z(t_{1g}) = (35Z/2r_0^6)xy(x^2-y^2) , \quad (19)$$

where r_0 is the chromium-ligand distance and Z is the nuclear charge. The required matrix element is then given by

$$\langle \zeta \mid V_z(t_{1g}) \mid v\rangle = (210\sqrt{2}Z/r_0^6) \times \sum_k \sum_l C_kC_l(\zeta_k\zeta_l)^{7/4}(\zeta_k+\zeta_l)^{11/2} . \quad (20)$$

Values or ν calculated from Eqs. (15) and (20) are listed in Table I. For want of better information, we have assumed that the chromium-ligand distance is one-quarter of the lattice parameter ($r_0=a_0/4$) and that the frequency of the t_{1g} promoting mode is the same as that of the a_{1g} accepting mode listed in Table III of I; the latter assumption is probably an overestimate. Bartram and Stoneham[16] have further emphasized the importance of orthogonalizing the pseudo-wave-function to occupied ligand core orbitals. This step has not been implemented in the present instance, and thus the calculated values of ν listed in Table I should be regarded as preliminary. However, it is evident that a value of ν of the order of 10^{15} sec^{-1} is a reasonable estimate for all three host crystals.

TABLE I. Values of the promoting-mode factor ν calculated from Eqs. (15) and (20), with the assumptions $r_0=a_0/4$ and $\omega_p=\omega_0$.

Host crystal	ν (10^{15} sec^{-1})
Cs_2NaYCl_6	0.33
K_2NaScF_6	1.04
K_2NaGaF_6	1.49

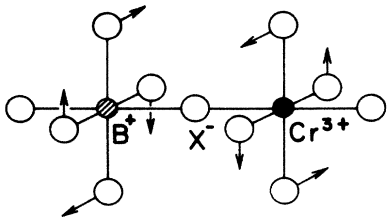

FIG. 1. Promoting mode of t_{1g} symmetry in ordered perovskite A_2BMX_6:Cr^{3+}.

IV. SINGLE-CONFIGURATION-COORDINATE, LINEAR-COUPLING MODEL

The special case of linear coupling to a single accepting mode (or, equivalently, to a set of degenerate modes) was investigated by Huang and Rhys.[2] In that case, the lineshape function $G(\Omega)$ in Eq. (12) can be evaluated in closed form,

$$G(\Omega) = \exp[-(2\bar{n}+1)S_0] \times \sum_{m=-\infty}^{\infty} [(\bar{n}+1)/\bar{n}]^{m/2} \times I_{|m|}(2S_0[\bar{n}(\bar{n}+1)]^{1/2})\delta(\Omega-m\omega_0) , \quad (21)$$

where

$$\bar{n} = [\exp(\hbar\omega_0/k_BT)-1]^{-1} , \quad (22)$$

ω_0 is the accepting-mode angular frequency and S_0 is the zero-temperature Huang-Rhys factor, illustrated schematically in Fig. 7 of I.

Several limiting cases are of interest. In weak coupling, $S_0 \ll 1$, typical of rare-earth impurities, the energy-gap law[5] applies:

$$W_{NR} \simeq \nu \exp(-\alpha p)(\bar{n}+1)^p/(2\pi p)^{1/2} , \quad (23)$$

$$\alpha = \ln(p/S_0) - 1 , \quad (24)$$

where $p(=\Omega_0/\omega_0)$ is the number of accepting-mode phonons required to bridge the energy gap between electronic states. In strong coupling, $S_0 \gg 1$, typical of F centers, thermally activated behavior[27] is predicted:

$$W_{NR} \simeq \nu[(2\bar{n}+1)/2\pi S_0]^{1/2} \exp(-E_A/k_B T^*) , \quad (25)$$

where

$$k_B T^* = (\hbar\omega_0/2)\coth(\hbar\omega_0/2k_B T) , \quad (26)$$

and where E_A is the curve-crossing energy with respect to the excited-state minimum, as shown in Fig. 7 of I. Equations (25) and (26) reduce approximately to the Mott formula[28] in the limit $k_B T \gg \hbar\omega_0$. (See the discussion in I.) Finally, in the limit $T=0$, the expression for W_{NR} simplifies to

$$W_{NR} = \nu \exp(-S_0) S_0^{p-1}/(p-1)! . \quad (27)$$

Unfortunately, none of these limiting cases is appropriate for transition-metal complexes where the coupling is intermediate, $S_0 \simeq 1$, and where radiationless transitions are important at intermediate temperatures, $k_B T \simeq \hbar\omega_0$. Accordingly, we have employed a smoothed approximation of Eq. (21) in Eq. (9), with parameters S_0, ω_0, and Ω_0 determined for low-field chromium complexes in ordered perovskites by moments analysis of fluorescence spectra. (See Table III of I.) The promoting-mode factor ν was adjusted to fit the experimental value of $\ln(\tau_{NR})[=-\ln(W_{NR})]$, inferred from lifetime data reported in I, at a single temperature for each host crystal. It can be seen from Fig. 2 that the predicted temperature dependence of $\ln(\tau_{NR})$ is in reasonable agreement with experiment. However, the adjusted values of ν listed in Table II are too large by a factor of 6—8 orders of magnitude, and are physically unreasonable. Put differently, the radiationless-transition rates predicted with the calculated value of ν are from 6—8 orders of magnitude smaller than the observed rates. Thus the failure of the single-configuration coordinate, linear-coupling model transcends the limitations of the Mott formula and compels a search for a more realistic model.

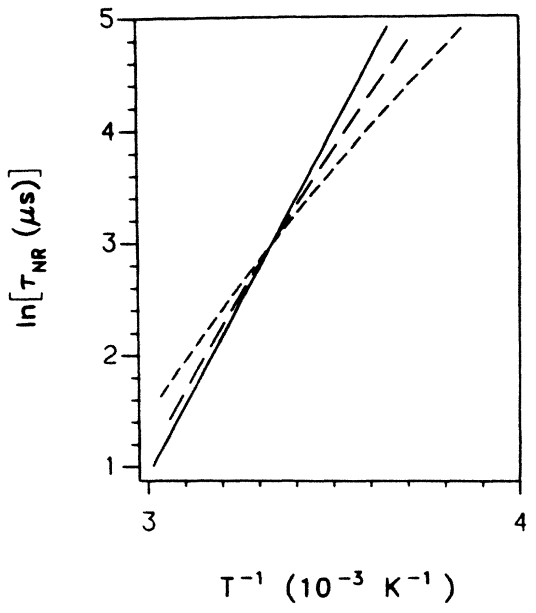

FIG. 2. Temperature dependence of the lifetimes of radiationless transitions in $Cs_2NaYCl_6:Cr^{3+}$. The solid line was obtained from the measured lifetime reported in I by subtracting the extrapolated radiative transition rate from τ^{-1}. Long-dashed and short-dashed lines are calculated from Eq. (9) with $G(\Omega)$ given, respectively, by Eq. (21) (single-configuration-coordinate, linear-coupling model) and Eq. (34) (multimode, linear-coupling model) for $\delta=0.3$. The promoting-mode factor was adjusted as indicated in Table II.

TABLE II. Values of the promoting-mode factor ν (sec^{-1}) determined by fitting values of $\ln(\tau_{NR})$ calculated on the single-configuration, linear-coupling model ($\delta=0$) and the multimode, linear-coupling model ($\delta>0$) to experimental values at the temperatures indicated.

δ	$CsNaYCl_6$[a]	K_2NaScF_6[b]	K_2NaGaF_6[c]
0.0	1.1×10^{23}	6.5×10^{21}	1.8×10^{21}
0.1	1.7×10^{22}	6.3×10^{20}	2.2×10^{20}
0.2	7.6×10^{22}	1.1×10^{21}	4.7×10^{20}
0.3	3.3×10^{24}	1.3×10^{22}	6.3×10^{21}

[a]300 K.
[b]550 K.
[c]650 K.

V. MULTIMODE LINEAR-COUPLING MODEL

The extremely slow radiationless-transition rate predicted for low-field chromium complexes by the single-configuration-coordinate, linear-coupling model is partly a consequence of the very large number of phonons required to bridge the energy gap in these systems. Accordingly, a model which takes account of the range of vibration frequencies would appear to be more promising. Such a model has been developed for the case of linear coupling[11] and has been applied with some success to a transition-metal complex.[10]

Since a closed-form expression for the normalized line-shape function $G(\Omega)$ is no longer available in the case of linear coupling to many modes with a range of frequencies, it is necessary to develop suitable approximations. The multimode problem was first considered by O'Rourke,[29] who showed that the Fourier transform of the line-shape function $G(\Omega)$ has the form

$$\Gamma(t) = \int_{-\infty}^{\infty} d\Omega \exp(i\Omega t) G(\Omega) = \exp[-S + g(t)] , \quad (28)$$

where

$$g(t)=\int_0^\infty d\omega\{[\bar{n}(\omega)+1]\exp(i\omega t) +\bar{n}(\omega)\exp(-i\omega t)\}A(\omega)\ , \tag{29}$$

$$S=\int_0^\infty d\omega[2\bar{n}(\omega)+1]A(\omega)\ , \tag{30}$$

and

$$\bar{n}(\omega)=[\exp(\hbar\omega/k_BT)-1]^{-1}\ . \tag{31}$$

The function $A(\omega)$ is the coupling constant per unit vibrational frequency range, and S is the temperature-dependent Huang-Rhys factor. Equations (28)—(31) provide the point of departure for the approximations of Pryce[11] and of Weissman and Jortner.[30]

Pryce[11] developed an expression for $G(\Omega)$ from the series expansion of $\exp[g(t)]$ in the inverse Fourier transform,

$$G(\Omega)=\exp(-S)\left[\delta(\Omega)+\sum_{n=1}^{\infty}(S^n/n!)B_n(\Omega)\right]\ , \tag{32}$$

where $B_n(\Omega)$ is the n-fold convolution of a normalized single-phonon side band given by

$$B_1(\Omega)=(S^{-1}/2\pi)\int_{-\infty}^{\infty}dt\exp(-i\Omega t)g(t)\ . \tag{33}$$

He then invoked the central-limit theorem to obtain an approximate expression for $B_n(\Omega)$ which exploits the smoothing effect of the n-fold convolution for large n. A difficulty with this approximation is that $B_1(\Omega)$ is bimodal at finite temperature, since it includes both absorption and emission of phonons; consequently, the approximation is adequate only for inconveniently large values of n.

The refinement of Weissman and Jortner[31] proceeds from an alternative expansion of the line-shape function which emphasizes the net number of phonons emitted. A major further simplification is achieved by replacing ω by its average value ω_0 in Eq. (31); this "narrow-coupling" approximation, which is justified for a relatively sharply peaked distribution $A(\omega)$, yields the approximate expression

$$G(\Omega)\simeq\exp[-(2\bar{n}+1)S_0] \times\sum_{m=-\infty}^{\infty}[(\bar{n}+1)/\bar{n}]^{m/2}I_{|m|}(2S_0[\bar{n}(\bar{n}+1)]^{1/2}) \times F(m+k_0,k_0,\Omega)\ , \tag{34}$$

where

$$F(m+k_0,k_0,\Omega)\simeq[2\pi(m+k_0)\sigma_0^2]^{-1/2} \times\exp[-(\Omega-m\omega_0)^2/2(m+2k_0)\sigma_0^2]\ , \tag{35}$$

$$k_0=[-m+(m^2+\alpha^2)^{1/2}]/2\ , \tag{36}$$

$$S_0=\int_0^\infty d\omega\,A(\omega)\ , \tag{37}$$

$$\omega_0=S_0^{-1}\int_0^\infty d\omega\,\omega A(\omega)\ , \tag{38}$$

$$\sigma_0^2=S_0^{-1}\int_0^\infty d\omega\,\omega^2A(\omega)-\omega_0^2\ , \tag{39}$$

and $\bar{n}$ is defined by Eq. (22). This expression for the line-shape function is essentially identical to that for the single-configuration-coordinate, linear-coupling model except that the δ function in Eq. (21) has been replaced by a normalized Gaussian function in Eq. (34) whose width increases with the net number of emitted phonons.

In principle, one can recover the distribution function $A(\omega)$ by deconvolution of resolved fluorescence spectra at low temperature.[31] However, the narrow-coupling approximation has the advantage that it involves only the zeroth, first, and second moments of $A(\omega)$; i.e., S_0, ω_0, and σ_0^2, respectively. These quantities in turn can be related to the second moment $N_2[\langle(\hbar\Omega)^2\rangle-\langle\hbar\Omega\rangle^2]$ of the complete line-shape function, as follows: The quantities $\langle\Omega^n\rangle$ can be derived from the Fourier-transformed line-shape function $\Gamma(t)$ by series expansion of $\exp(i\Omega t)$ in Eq. (28),

$$\langle\Omega^n\rangle=[\partial^n\Gamma(t)/\partial(it)^n]_{t=0}\ . \tag{40}$$

The right-hand side of Eq. (40) can then be evaluated with the help of Eq. (29) to yield the relation

$$N_2=S_0\hbar^2(\omega_0^2+\sigma_0^2)\coth(\hbar\omega_0/2k_BT)\ . \tag{41}$$

Comparison with Eq. (8) of I reveals that the empirical quantities S_0 and ω_0 listed in Table III of I can be reinterpreted as $S_0(1+\delta)$, where

$$\delta=\sigma_0^2/\omega_0^2\ , \tag{42}$$

and the mean phonon frequency ω_0 defined by Eq. (38), respectively.

Radiationless-transition rates were calculated as a function of temperature by incorporating Eqs. (34)—(39) in Eq. (9). The parameters $S_0(1+\delta)$ and ω_0 were determined from Table III of I. Calculations were performed for a range of values of δ, and for each value the promoting-mode factor ν was adjusted to fit the experimental value of $\ln(\tau_{NR})$ at a single temperature for each host crystal. It is evident from Table II that no significant improvement in ν was achieved relative to the single-configuration-coordinate, linear-coupling model ($\delta=0$) presented in Sec. V; the advantage provided by a range of phonon frequencies was offset by the reduction of S_0. Furthermore, the slope of $\ln(\tau_{NR})$ versus T^{-1} was diminished, as illustrated in Fig. 2 for Cs_2NaYCl_6:Cr^{3+}; essentially similar curves were obtained for the other two host crystals, and in each case, $\delta=0$ corresponds best with the experimentally determined activation energy. Thus we are forced to conclude that the multimode linear-coupling model also fails to explain the observed high radiationless-transition rate of low-field chromium complexes in ordered perovskites.

VI. TWO-COORDINATE, QUADRATIC-COUPLING MODEL

The preceding sections attest the failure of models based on linear coupling to modes of a_{1g} symmetry to explain radiationless transitions in low-field chromium complexes, even when extended to include a range of vibration frequencies. Such a linear-coupling model was applied with some success to Co^{2+} in $KMgF_3$ by Sturge,[10] who attributed a residual discrepancy to anharmonicity. Al-

though anharmonicity could be entertained as an *ad-hoc* hypothesis to explain the much larger discrepancy in the present case as well, we have sought an alternative explanation within the harmonic approximation.

An obvious extension of the single-configuration-coordinate model is the inclusion of quadratic coupling; i.e., the assumption of different vibration frequencies in different electronic states. Line shapes corresponding to pure quadratic coupling have been discussed by Keil,[32] and the method of Struck and Fonger,[33] in which vibrational overlap integrals are evaluated numerically, permits computation of line shapes for combined linear and quadratic coupling. However, quadratic coupling to a_{1g} modes is expected to be relatively weak for chromium complexes, on the basis both of the Tanabe-Sugano diagram[34] and of the observed symmetry of absorption and emission lines. (The transformation from the Tanabe-Sugano diagram to a configuration-coordinate diagram necessarily introduces both quadratic coupling and anharmonicity, which were neglected in I. However, these effects are much too small to account for the observed radiationless-transition rates.) The degree of quadratic coupling to the a_{1g} mode in $K_2NaGaF_6:Cr^{3+}$ is known from the resolved vibronic structure of low-temperature absorption and fluorescence spectra;[35] the a_{1g}-mode frequencies in the $^4T_{2g}$ and $^4A_{2g}$ states are, respectively, 556 cm^{-1} and 568 cm^{-1}. It was established by numerical line-shape simulation that an enhancement of the radiationless-transition rate by less than 2 orders of magnitude can be expected from this degree of quadratic coupling.

The model can be further extended to include coupling to accepting modes of lower symmetry. Distortions of the seven-atom octahedron which are even under inversion include symmetry-adapted displacements of a_{1g}, e_g, and t_{2g} symmetry. Optical absorption and emission spectra with resolved vibronic structure, together with Raman spectra, provide evidence for appreciable coupling to e_g and t_{2g} modes as well as to a_{1g} modes.[35–38] Both linear coupling (Jahn-Teller effect) and quadratic coupling to low-symmetry modes are expected. The Tanabe-Sugano diagram no longer suffices to characterize the system; when spin-orbit coupling is neglected, a complete description of the $^4A_{2g}$ and $^4T_{2g}$ electronic states involves four adiabatic-potential-energy surfaces in a six-dimensional configuration-coordinate space.

The additional degrees of freedom in this extended model provide alternative possibilities for radiationless-transition mechanisms. In particular, it is found that a t_{2g} distortion effects a profound reduction in crystal-field splitting, which is manifest as strong quadratic coupling. The reason for this reduction is apparent from a qualitative comparison of the electronic wave functions for maximum spin projection,[39]

$$\psi(t_2^3\,{}^4A_2, M=\tfrac{3}{2}) = -|\overset{+}{\xi}\overset{+}{\eta}\overset{+}{\zeta}| \tag{43}$$

and

$$\psi(t_2^2({}^3T_1)e\,{}^4T_2, M=\tfrac{3}{2}, \zeta) = -|\overset{+}{\xi}\overset{+}{\eta}\overset{+}{v}| \ . \tag{44}$$

The Slater determinants on the right-hand sides differ in only one orbital, $t_{2g}(\zeta)$ in the ground state, and $e_g(v)$ in the excited state. These two orbitals are illustrated in Fig. 3, where it can be seen that the lobes of the $t_{2g}(\zeta)$ orbital in the $^4A_{2g}$ state avoid the ligands, whereas those of the $e_g(v)$ orbital in the $^4T_{2g}$ state are directed toward the ligands. This difference is the source of the crystal-field splitting, and it is evident from Fig. 3 that a $t_{2g}(\zeta)$ displacement enhances the energy of the ζ orbital and diminishes that of the v orbital, independent of its sign. Thus the elastic constant is enhanced in the ground state and diminished in the excited state, with consequent quadratic coupling. The $t_{2g}(\zeta)$ distortion is linearly coupled to the ξ and η orbital components of the $^4T_{2g}$ state, as well, but that (Jahn-Teller) coupling is estimated to be weaker than linear coupling to the a_{1g} displacement.

In order to render the model more tractable and to isolate its essential features, we have adopted a simplified version in which we have restricted consideration to the a_{1g} coordinate plus one $t_{2g}(\zeta)$ coordinate, and to the $^4A_{2g}$ electronic state plus the ζ-orbital component of the $^4T_{2g}$ state; i.e., to two adiabatic-potential-energy surfaces in a two-dimensional configuration-coordinate space. The simplified model is illustrated in Fig. 4.

The adiabatic potential energies in a point-ion approximation are given by

$$E({}^4A_{2g}) = -12Dq + 5Dq[1-\cos(4\psi)] + M\omega_\xi^2 Q_\xi^2/2 \ , \tag{45}$$

$$E({}^4T_{2g}\zeta) = -2Dq - 5Dq[1-\cos(4\psi)] + M\omega_\xi^2 Q_\xi^2/2 \ , \tag{46}$$

where

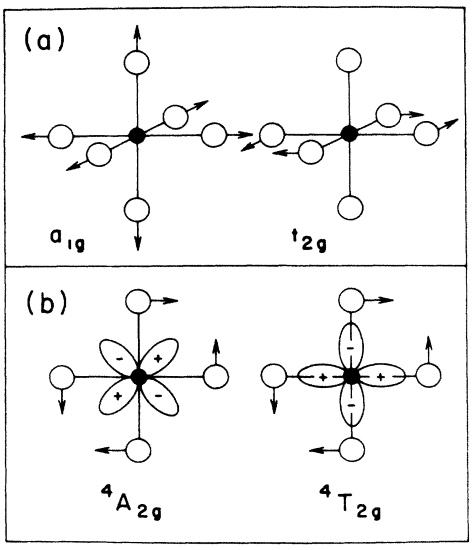

FIG. 3. (a) a_{1g} and $t_{2g}(\zeta)$ displacements of ligands in an octahedral chromium complex. (b) $t_{2g}(\zeta)$ orbital in $^4A_{2g}$ state and $e_g(v)$ orbital in $^4T_{2g}$ state. It can be seen that the energy of the former is increased and that of the latter is decreased by a $t_{2g}(\zeta)$ displacement.

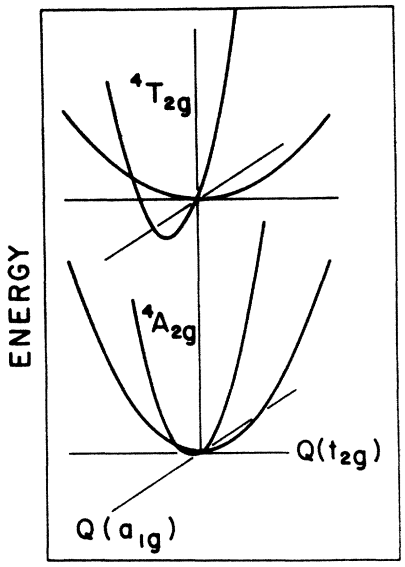

FIG. 4. Two-configuration-coordinate model with linear coupling to an a_{1g} mode and quadratic coupling to a $t_{2g}(\zeta)$ mode. Only the ζ orbital component of the $^4T_{2g}$ electronic state is retained in the model.

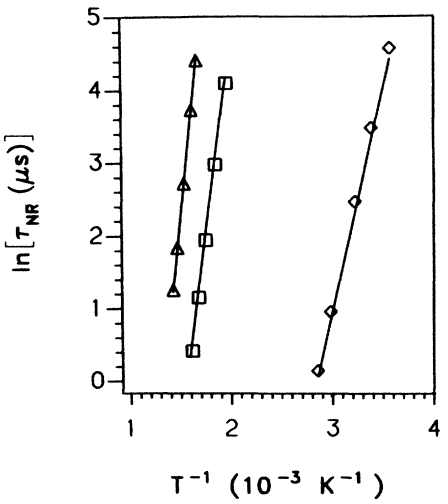

FIG. 6. Temperature dependence of the lifetime of radiationless transitions in Cs_2NaYCl_6 (◇), K_2NaScF_6 (□), and K_2NaGaF_6 (△), calculated from Eq. (9) and from simulated line shapes for the two-configuration-coordinate model with parameters adjusted for a least-squares fit. Solid lines were obtained from the measured lifetimes reported in I by subtracting the extrapolated radiative transition rate from τ^{-1}.

$$\psi=\tan^{-1}(Q_\zeta/2r_0)\ , \tag{47}$$

$$Dq=Dq_0[1+(Q_\zeta/2r_0)^2]^{-5/2}\ , \tag{48}$$

the elastic potential energy has been added to the right-hand side of Eqs. (45) and (46), M is the mass of one halogen ion, $Q_\zeta/2$ is its displacement, and r_0 is the nearest-neighbor distance. In the harmonic approximation, Eqs. (45) and (46) reduce to

$$E(^4A_{2g})\simeq -12Dq_0+M\omega_f^2Q_\zeta^2/2 \tag{49}$$

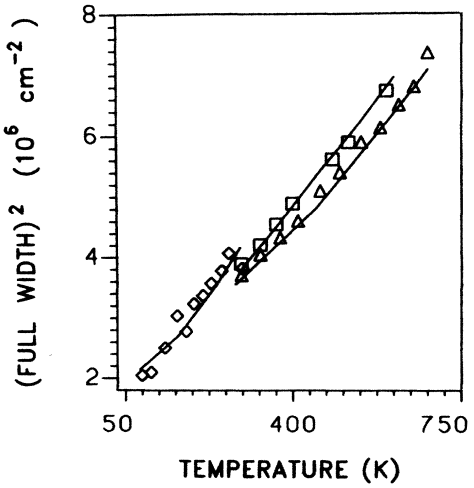

FIG. 5. Temperature dependence of the square of the full width at half maximum of chromium fluorescence spectra in Cs_2NaYCl_6 (◇), K_2NaScF_6 (□), and K_2NaGaF_6 (△). Solid lines are from simulated line shapes for the two-configuration-coordinate model, with parameters adjusted for a least-squares fit.

and

$$E(^4T_{2g},\zeta)\simeq -2Dq_0+M\omega_i^2Q_\zeta^2/2\ , \tag{50}$$

where

$$\omega_f^2=\omega_i^2+105Dq_0/2Mr_0^2\ . \tag{51}$$

Line shapes for quadratic coupling to the t_{2g} mode and linear coupling to the a_{1g} mode were simulated numerically by the method of Struck and Fonger,[33] which exploits the Manneback[40] recursion relations for vibrational overlap integrals. Contributions to $G(\Omega)$ were accumulated in frequency intervals of width ω_0, the frequency of the a_{1g} mode. It follows from Eq. (12) that the composite line shape is a convolution of linear and quadratic com-

TABLE III. Adjusted parameters for the two-configuration-coordinate, linear- and quadratic-coupling model. Values inferred from resolved vibronic structure of low-temperature spectra are shown in parentheses for comparison.

	Cs_2NaYCl_6	K_2NaScF_6	K_2NaGaF_6
S_0	6.86	3.50	3.12
$\hbar\Omega_0$ (cm^{-1})	11 500	13 750	13 950
$\hbar\omega_0$ (cm^{-1})	230 (300)[a]	369	393 (568)[b]
$\hbar\omega_f$ (cm^{-1})	120 (139)[c]	243	297 (234)[c]
ν (10^{15} sec^{-1})	1.4	0.9	24.0
$\hbar\omega_i$ (cm^{-1})[d]	73	161	218

[a]R. W. Schwartz, Inorg. Chem. **15**, 2817 (1976).
[b]J. Ferguson, H. J. Guggenheim, and D. L. Wood, J. Chem. Phys. **54**, 504 (1971).
[c]H. V. Güdel and T. R. Snellgrove, Inorg. Chem. **17**, 1617 (1978) (for $Cs_2NaInCl_6$).
[d]Calculated from Eq. (51); not independently adjusted.

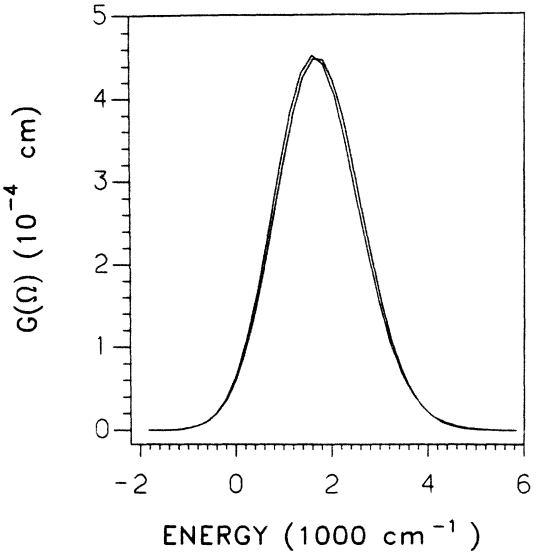

FIG. 7. Comparison of simulated fluorescence line shapes of $Cs_2NaYCl_6:Cr^{3+}$ at 300 K for the single-configuration-coordinate model and the two-configuration-coordinate model with parameters optimized in each case. The line shapes are virtually indistinguishable, and both agree equally well with experiment.

ponents; the required convolution integral was performed numerically. The parameters of this model include the zero-temperature Huang-Rhys factor S_0 and vibration frequency ω_0 of the a_{1g} mode, the ground-state vibration frequency ω_f of the t_{2g} mode, and the promoting-mode factor ν; the same number as for the multimode, linear-coupling model. The temperature dependence of the square of the full width at half maximum of the composite line shape was fit to empirical data from the fluorescence spectra reported in I, as shown in Fig. 5; this quantity was employed rather than the second moment, because it could be determined more precisely from measured fluorescence spectra. The temperature dependence of W_{NR} from Eq. (9) was simultaneously fit to the measured values of τ_{NR}^{-1}, reported in I, as shown in Fig. 6. The adjusted values of the parameters are listed in Table III, where they are compared with independently determined values.

It is evident that the optimum values of the promoting-mode factors ν in Table III are in far better agreement with the calculated values in Table I than are those for the multimode linear-coupling model in Table II. Optimum values of the ground-state t_{2g} vibration frequencies ω_f compare favorably with values derived from

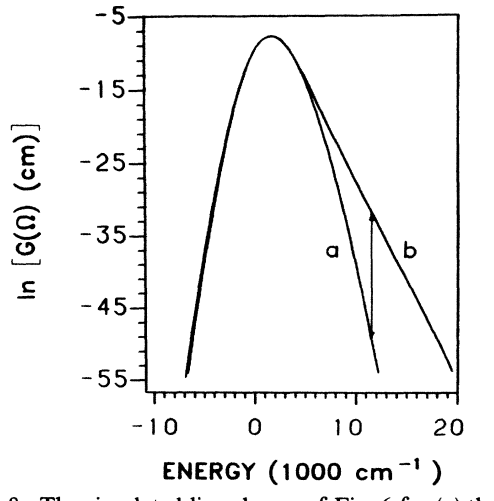

FIG. 8. The simulated line shapes of Fig. 6 for (a) the single-configuration-coordinate model and (b) the two-configuration-coordinate model, compared on a semi-log scale. Although the line shapes are virtually indistinguishable in the range of frequencies accessible to direct observation, they differ by eight orders of magnitude at the frequency Ω_0 corresponding to the gap energy.

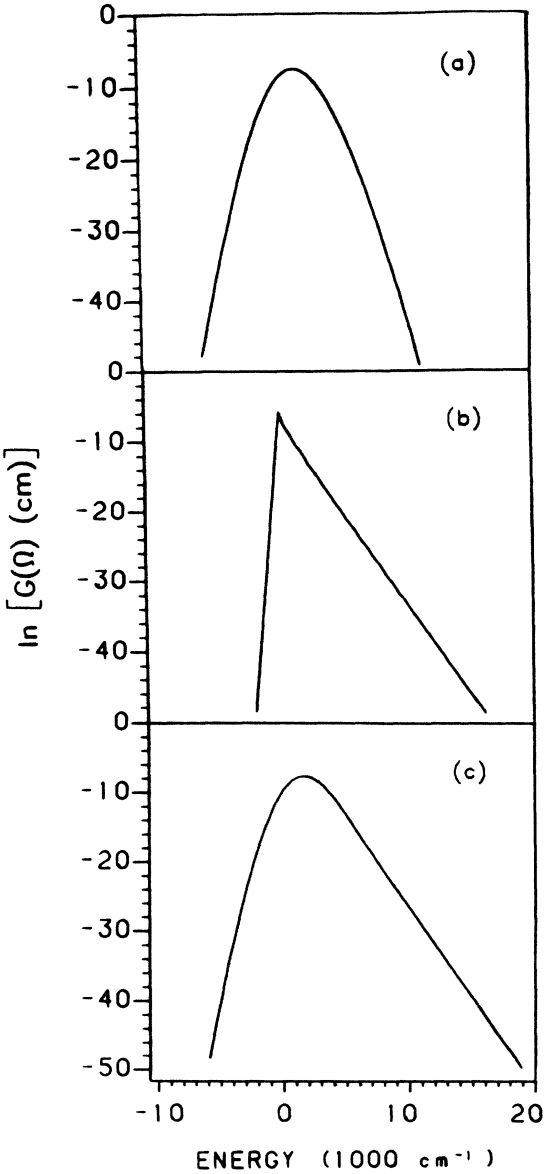

FIG. 9. Components of the simulated line-shape function for the two-configuration-coordinate model. (a) Line-shape function for linear coupling to the a_{1g} mode. (b) Line-shape function for quadratic coupling to the t_{2g} mode. (c) Composite line-shape function obtained by numerical convolution of (a) and (b).

vibronic structure of low-temperature spectra. The a_{1g} vibration frequencies ω_0 are considerably less than those derived from vibronic structure, but are comparable with the values determined for the single-configuration-coordinate, linear-coupling model in I; as in that case, ω_0 is an effective frequency which incorporates contributions of both lattice modes and resonances of a_{1g} and e_g symmetry. Thus the two-coordinate, quadratic-coupling model is in substantial quantitative agreement with all of the available data.

VII. DISCUSSION AND CONCLUSIONS

The data presented in I on the temperature dependence of fluorescence lifetimes and spectra of low-field chromium complexes in ordered perovskites serve to characterize both radiationless-transition rates and adiabatic-potential-energy surfaces. We have investigated several theoretical models in an effort to provide a consistent quantitative explanation of these data. Models based on linear coupling to a_{1g} modes were found to fail by many orders of magnitude to explain observed transition rates when constrained by empirical spectral information. The success of the two-coordinate, linear- and quadratic-coupling model within the harmonic approximation can be understood from consideration of Figs. 7 and 8. The simulated line shape of the single-configuration-coordinate, linear-coupling model is compared with the composite line shape for the two-coordinate, linear- and quadratic-coupling model in Fig. 7. Parameters were adjusted in both cases to fit the temperature dependence of the square of the full width at half maximum. The two line shapes appear to be virtually indistinguishable over that part of the energy range which is accessible to direct observation, and either one is in satisfactory agreement with the measured fluorescence spectrum. Comparison of the same two line shapes on a semi-log scale over a wider energy range, as shown in Fig. 8, is much more revealing. The two line-shape functions differ by many orders of magnitude at the gap energy, $\hbar\Omega_0$, far beyond the range of measurable spectra, thus accounting for the differences in predicted radiationless-transition rates. The origin of this difference can be understood from a semiclassical model[41] in which the line-shape function for linear coupling is approximately Gaussian, while that for quadratic coupling is approximately exponential. The quantum-mechanical line shapes are similar, and thus are approximately parabolic and linear, respectively, on a semi-log scale. It is evident from Fig. 9 that the linear tail characteristic of quadratic coupling is preserved in the convolution of line-shape functions in the two-coordinate model, with consequent enhancement of the radiationless-transition rate. The sensitivity of thermal fluorescence quenching to constituents beyond the immediate ligands now finds qualitative explanation in the influence of those constituents on the t_{2g}-mode frequency, ω_f.

ACKNOWLEDGMENT

This investigation was supported by U.S. Army Research Office Contract No. DAAG29-82-K-0158.

*Present address: Department of Chemistry, Boston University, Boston, MA 02215.

[1]L. J. Andrews, A. Lempicki, B. C. McCollum, C. J. Giunta, R. H. Bartram, and J. F. Dolan, Phys. Rev. B **34**, 2735 (1986).
[2]K. Huang and A. Rhys, Proc. R. Soc. (London) Ser. A **204**, 406 (1950).
[3]A. M. Stoneham, *Theory of Defects in Solids* (Clarendon, Oxford, 1975), pp. 477–547.
[4]R. Englman, *Non-Radiative Decay of Ions and Molecules in Solids* (North-Holland, Amsterdam, 1979).
[5]L. A. Riseberg and H. W. Moos, Phys. Rev. **174**, 429 (1968).
[6]H. V. Lauer and F. K. Fong, J. Chem. Phys. **60**, 274 (1974).
[7]R. Englman and B. Barnett, J. Lumin. **3**, 37 (1970).
[8]W. H. Fonger and C. W. Struck, Phys. Rev. B **11**, 3251 (1975).
[9]K. Tamimura, W. A. Sibley, and L. G. DeShazer, Phys. Rev. B **31**, 3980 (1985).
[10]M. D. Sturge, Phys. Rev. B **8**, 6 (1973).
[11]M. H. L. Pryce, in *Phonons,* edited by R. W. H. Stevenson (Plenum, New York, 1966).
[12]R. H. Bartram, in *Tunable Solid State Lasers,* edited by P. Hammerling, A. B. Budgor, and A. Pinto (Springer-Verlag, Berlin, 1985), pp. 155–163.
[13]L. J. Andrews, A. Lempicki, and B. C. McCollum, Chem. Phys. Lett. **74**, 404 (1980).
[14]M. Bixon and J. Jortner, J. Chem. Phys. **50**, 4061 (1969).
[15]S. H. Lin and R. Bersohn, J. Chem. Phys. **48**, 2732 (1968).
[16]R. H. Bartram and A. M. Stoneham, J. Phys. C **18**, L549 (1985).
[17]G. Helmis, Ann. Phys. (Leipzig) **19**, 41 (1956).
[18]R. Pässler, Czech. J. Phys. B **24**, 322 (1974); **32**, 246 (1982).
[19]K. Huang, Sci. Sin. **24**, 27 (1981).
[20]E. Gutsche, Phys. Status Solidi B **109**, 583 (1982).
[21]M. G. Burt, J. Phys. C **16**, 4137 (1983).
[22]A. Lentz, J. Phys. Chem. Solids **35**, 827 (1974).
[23]J. S. Griffith, *The Theory of Transition Metal Ions* (Cambridge University Press, Cambridge, England, 1961).
[24]M. Weissbluth, *Atoms and Molecules* (Academic, New York, 1978), p. 159–167.
[25]P. J. Hay, J. Chem. Phys. **66**, 4377 (1977).
[26]B. S. Gourary and A. E. Fein, J. Appl. Phys. **33**, 331 (1962).
[27]R. Englman and J. Jortner, Mol. Phys. **18**, 145 (1970).
[28]N. F. Mott, Proc. R. Soc. London Ser. A **167**, 384 (1938).
[29]R. C. O'Rourke, Phys. Rev. **91**, 265 (1953).
[30]Y. Weissman and J. Jortner, Philos. Mag. B **37**, 24 (1978).
[31]P. Giesecke, W. Von der Osten, and U. Röder, Phys. Status Solidi B **51**, 723 (1972).
[32]T. H. Keil, Phys. Rev. **140**, A601 (1965).
[33]C. W. Struck and W. H. Fonger, J. Lumin. **10**, 1 (1975).
[34]S. Sugano, Y. Tanabe, and H. Kamimura, *Multiplets of Transition-Metal Ions in Crystals* (Academic, New York, 1970), p. 109.
[35]J. Ferguson, H. J. Guggenheim, and D. L. Wood, J. Chem. Phys. **54**, 504 (1971).
[36]P. Greenough and A. G. Paulusz, J. Chem. Phys. **70**, 1967

(1979).
[37]R. W. Schwartz, Inorg. Chem. **15**, 2817 (1976).
[38]H. U. Güdel and T. R. Snellgrove, Inorg. Chem. **17**, 1617 (1978).
[39]S. Sugano, Y. Tanabe, and H. Kamimura, *Multiplets of Transition-Metal Ions in Crystals,* Ref. 34, pp. 66–76.
[40]C. Manneback, Physica (Utrecht) **17**, 1001 (1951).
[41]M. Lax, J. Chem. Phys. **10**, 1752 (1952).